MICROSCOPIC RELATIVISTIC DESCRIPTION OF NUCLEON-NUCLEUS SCATTERING

C.J. Horowitz and D. Murdock
Center for Theoretical Physics and Department of Physics
Massachusetts Institute of Technology
Cambridge, Massachusetts 02139

INTRODUCTION

A number of relativistic approaches to nuclear physics all suggest the optical potential or self-energy for a nucleon involves very large attractive Lorentz scalar and repulsive vector contributions. Relativistic mean field calculations[1] relate these potentials to large scalar (sigma) and vector (omega) meson couplings and provide a good description of charge densities for closed shell nuclei. Dirac optical model fits to elastic proton scattering[2] also use strong potentials to reproduce analyzing power data. Finally, relativistic impulse approximation (RIA) calculations[3] find strong potentials coming from large scalar and vector pieces of a Lorentz invariant representation of the NN amplitudes. These RIA calculations provide an excellent description of elastic scattering at energies of 500 MeV and above.

In this paper, microscopic relativistic optical potentials are calculated at energies near 200 MeV for elastic proton scattering from closed shell nuclei. The 200 Mev energy region is interesting for several reasons. First, as a bridge between high energies, where a simple impulse approximation is valid, and relativistic nuclear structure calculations. In this energy range one can examine the onset of medium modifications to the free NN interaction. Second, some nonrelativistic optical models show non Wood-Saxon potential shapes. These interesting shapes can be explained by quadratic potential terms resulting from a 2nd order reduction of the Dirac equation. Finally, there exists new spin rotation function (Q) data from IUCF[9] for proton elastic scattering from ^{12}C, ^{16}O, ^{40}Ca and ^{48}Ca at 200 MeV. Thus, with A_y and $d\sigma/d\Omega$ already measured one can compare theory to a complete set of scattering observables.

We begin by identifying the optical potential with the self-energy calculated in relativistic Brueckner theory. Here the ladder diagrams of a meson-nucleon field theory are summed self-consistently for two nucleons in the medium. Although this program has not yet been carried out completely the present calculations still contain important physics beyond the original RIA.

First, the original RIA representation of the NN amplitudes involve ambiguities which become increasingly serious as the energy is decreased. To resolve these ambiguities, a simple direct plus exchange model of the NN amplitudes [4] is employed which allows the use of a pseudovector ($\not{q}\gamma_5$ rather than simply γ_5) πN coupling. Next, medium modifications from Pauli blocking are included by using nuclear matter calculations in a local density approximation.

Section II describes the formalism for these calculations while section III shows results which quantitatively reproduce all measured spin observables (both A_y and spin rotation function Q) for closed shell nuclei. Finally, these calculations are compared to relativistic results of Tjon and Wallace [5] and the nonrelativistic calculations of Rikus and von Geramb [6] and section IV presents conclusions.

FORMALISM

Work is underway to develop a relativistic Brueckner formalism to include NN correlations in a meson-nucleon field theory[15]. Here a reaction matrix Γ (or G matrix) is introduced which sums the ladder diagrams between two nucleons in the medium. The reaction matrix satisfies a relativistic Brueckner Bethe Goldstone (RBBG) equation which is a generalization of the nonrelativistic result. This equation can be solved in the NN center of velocity frame and the results expressed as five Lorentz invariants (see below) which are easy to transform to the nuclear rest frame. Summing this interaction over the occupied states of the target (in its rest frame) gives the self-energy or optical potential (U_{opt}) which contains complex Lorentz scalar and vector pieces.

$$U_{opt}(1) = \sum_{2}^{occ} < 12|\Gamma|12 - 21 > \qquad (1)$$

Here 1 is the state of the projectile and 2 is an occupied target state ($|12 - 21>$ indicates an antisymmeterized matrix element).

There are two effects of the medium on the calculation of Γ . First, the Pauli principle limits the scattering to intermediate states above the Fermi sea. This Pauli blocking effect is included as described below. Second the nucleons should move in an average potential (given by the real part of eq. (1)). Such binding energy corrections change the free relationship between momentum and energy and enhance the lower components of the nucleon Dirac spinors.

We would like to examine these effects step by step so we include Pauli blocking but not binding energy corrections in these first calculations. Binding energy corrections are not expected to be large near 200 Mev since the real part of the nonrelativistic optical potential is small at this energy. However, binding E corrections may be larger at lower energies and will be included in future calculations.

In general, Γ is a complicated 4 x 4 $\otimes$ 4 x 4 Dirac matrix in the spinor spaces of the two nucleons. In principle a complete solution of the RBBG equation would determine this complex 256 component matrix, (Tjon and Wallace have calculated this complete matrix but only in the zero density limit[5]). It is much easier to simply solve the RBBG equation for its positive energy spinor matrix elements and make a model for the full matrix structure. Furthermore since these spinor matrix elements should reduce to the experimental NN amplitudes at zero density we will take these from data and only calculate the ratio of Pauli blocked to free NN interactions.

To construct an optical potential in a relativistic "tρ " approximation one must make important assumptions regarding the "off-shell" behavior of the NN amplitudes. First, Dirac spinor matrix elements of an operator $\hat{F}$ are equated to experimental amplitudes. The standard representation of $\hat{F}$ is

$$\hat{F} = \sum_i F_i \ (q, E) \ \lambda_1^i \ . \ \lambda_2^i$$

i		λ^i
s	(Scalar)	1
v	(Vector	γ^μ
p	(Pseudoscalar	γ^5
a	(Axial Vector)	$\gamma^5\gamma^\mu$
t	(Tensor)	$\sigma^{\mu\nu}$

(2)

Here λ_1^i is a Dirac operator in the spinor space of particle one and the Lorentz invariant amplitudes F_i are functions of energy E and momentum transfer q. We emphasize, only the free spinor matrix elements of eq. (2) are determined by the NN data while the full "off-shell" operator is needed to construct an optical potential.

To resolve ambiguities in the operator $\hat{F}$ a simple model which includes the direct and exchange first Born contributions from a number of mesons was developed.[4] This model divides the Lorentz invariant amplitudes into direct $\tilde{t}^D$ and exchange $\tilde{t}^X$ contributions

$$F_i \ (q) = \tilde{t}_i^D(q) + \tilde{t}_i^X(Q).$$

Here, the exchange momentum transfer Q is for scattering angle $\pi - \theta$. The exchange contributions to the scalar and vector invariants $\tilde{t}_s^X$, $\tilde{t}_v^X$ have important contributions from one pion exchange. As discussed in [4], it is important to evaluate these contributions using a pseudo<u>vector</u> ($\not{q}\gamma_5$) invariant in place of the pseudo<u>scalar</u> γ_5 in eq. (2). This serves to decrease (the effects of $\tilde{t}_s^X$ and $\tilde{t}_v^X$ substantially, at low energies. Note, the original RIA implicitly uses a pseudo<u>scalar</u> π N coupling.

The scalar i=s and vector i=v optical potentials U_i are calculated by folding t with ρ and making a local density approximation for the exchange term.

$$U_i \ (r) = -4 \ \pi i \frac{p}{M} \int d^3 s \ \Big\{ t_i^D \ (s) \quad \rho_i (\vec{r} + \vec{s}) + j_0 \ (ps) \ t_i^X (s) \ \rho_i \ (\vec{r} + \frac{1}{2} \vec{s}) \ \rho_{off} \ (k_F s) \Big\} \tag{3}$$

Here, p is the projectile momentum, j_0 (ps) a local density approximation to the projectile wavefunction, the off diagonal density matrix has been approximated by its nuclear matter value $\rho_{off}(ks) = \frac{3}{(sk)^3}(\sin(sk) - sk\cos(sk))$ and the local Fermi momentum k_F deduced from $\rho_v(\vec{r} + \frac{1}{2}\vec{s})$.[11] The baryon ρ_v and the scalar ρ_s densities are taken from mean field calculations [1] and have not been varied. Finally, t^X and t^D are fourier transforms of $\tilde{t}^X, \tilde{t}^D$.

It remains to include medium modifications from Pauli blocking. Nuclear matter calculations of the lowest order relativistic Brueckner optical potentials have been performed both with and without the Pauli operator. These calculations started with the HEA[8] one boson exchange potential and will be described in a latter work (they do not include binding E corrections). From the ratio of two nuclear matter calculations we define Pauli blocking correction factors a_i which can be applied to the finite nucleus optical potential in a local density approximation.

$$U_i(r) \Leftarrow \left\{1 - a_i(E) \left[\frac{\rho_v(r)}{\rho_0}\right]^{\frac{2}{3}}\right\} U_i(r) \qquad (4)$$

Here, $\rho_0 = .19\ fm^{-3}$ and the k_F^2 density dependence is based on simple phase space arguments. At E = 200 MeV, the nuclear matter calculations give

	Scalar		Vector		
	real	imag	real	imag	
a_i	-.01	.10	.06	.21	(5)

The calculation can be summarized as follows. Ref. [4] is used for the t matrix which is folded with the mean field densities of [1] and then multiplied by the Pauli blocking corrections of eq. (4) and (5).

RESULTS

Figure (1) shows the scalar and vector optical potentials for ^{40}Ca at 200 MeV. These agree well with phenomenological Dirac Wood-Saxon fits to the elastic data. Figure (2) shows the Schrödinger-like equivalent potential, U_{eff} for ^{208}Pb. Compared to the nonrelativistic Paris G matrix calculate of [6], we have a non-Wood-Saxon shape for the central and a much stronger real spin-orbit potential.

Figure (3) shows the cross section for ^{40}Ca. The use of pseudoscalar rather than pseudovector NN amplitudes leads to too high a cross section, while omitting the Pauli blocking corrections also overestimates σ and gives too much structure. The original RIA corresponds to both omitting Pauli blocking and using pseudoscalar amplitudes and would lead to a curve above all of these shown in figure (3). A full folding of the density dependence instead of the simple eq. (4) may improve the structure in the cross section. The analyzing power A_y (both TRIUMF and IUCF data) and the new preliminary IUCF spin rotation Q data [9] are shown for ^{40}Ca, ^{16}O and ^{48}Ca in Figures (4 - 6). The calculations agree very well with the data if Pauli blocking is included and pseudovector amplitudes are used.

Our calculations essentially agree with Tjon and Wallace[5] for the pseudovector NN amplitudes and for the spin observables in ^{40}Ca. However, these authors don't include Pauli blocking which may explain their overestimation of the cross section.

The effect of the Lorentz tensor potential is seen in Figure (6) to be very small. All of the other calculations shown omit this term.

For the heavier nuclei, Q has not yet been measured but A_y is shown in Figures (7) and (8) for ^{90}Zr and ^{208}Pb. For Pb, the nonrelativistic calculation of Ref. [6] is seen to underestimate the depth of the minima in A while the relativistic results are very good for both Zr and Pb.

The energy dependence of various corrections is examined with calculations for ^{208}Pb at 400 MeV. At this energy there is almost no difference between pseudovector and pseudoscalar NN amplitudes. In addition the effects of Pauli blocking are very small. Figure (9) shows the analyzing power in ^{208}Pb. Calculations including Pauli

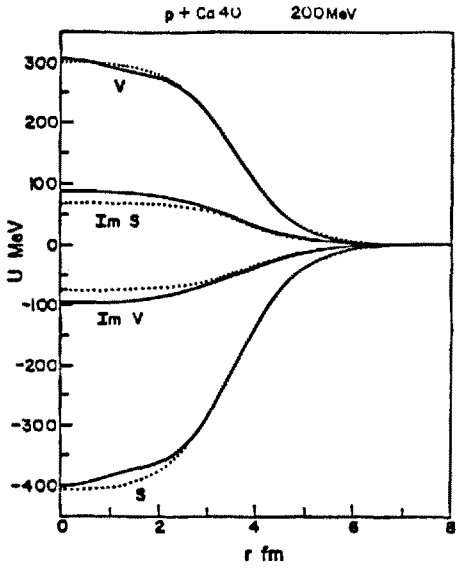

Fig. 1. Relativistic optical potentials for ^{40}Ca (solid). Dotted lines are phenomenological fits.[2,10]

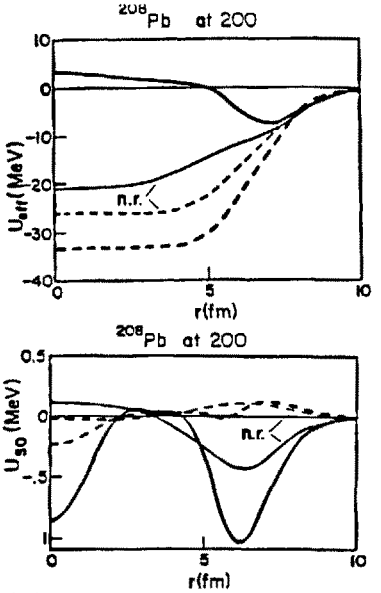

Fig. 2. (a) shows Schrodinger-like equivalent central pot. for ^{208}Pb (solid = real and dotted = imaginary part.) The non-relativistic (n.r.) curves are from 6. (b) as (a) but for spin orbit potential.

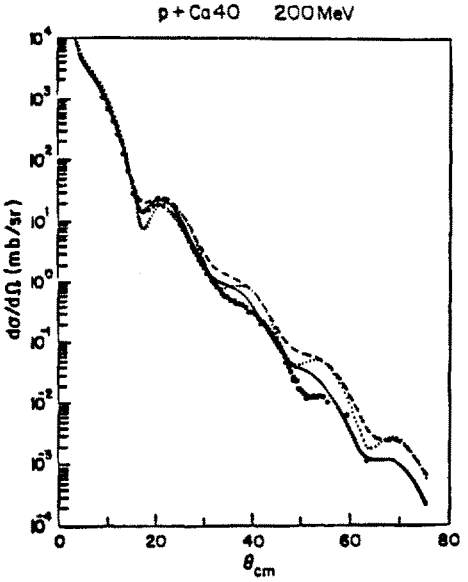

Fig. 3. Cross section for ^{40}Ca (solid). The dashed curve uses pseudoscalar rather than pseudovector NN amplitudes and the dotted curve omits Pauli-blocking (data from IUCF and TRIUMF[9]).

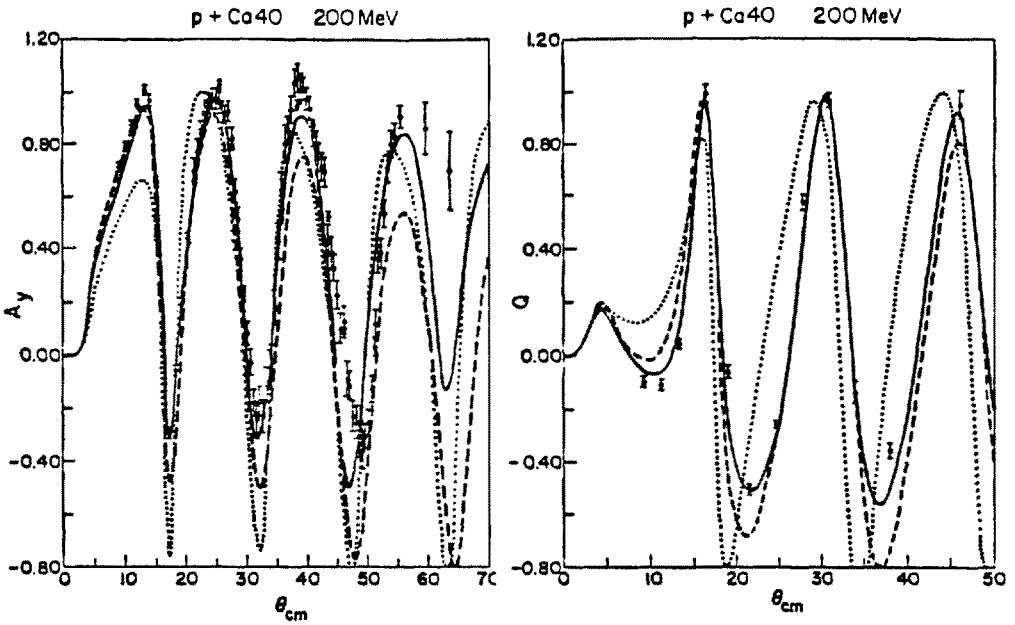

Fig. 4. Spin observables A_y and Q for ^{40}Ca, see caption to Fig. 3.

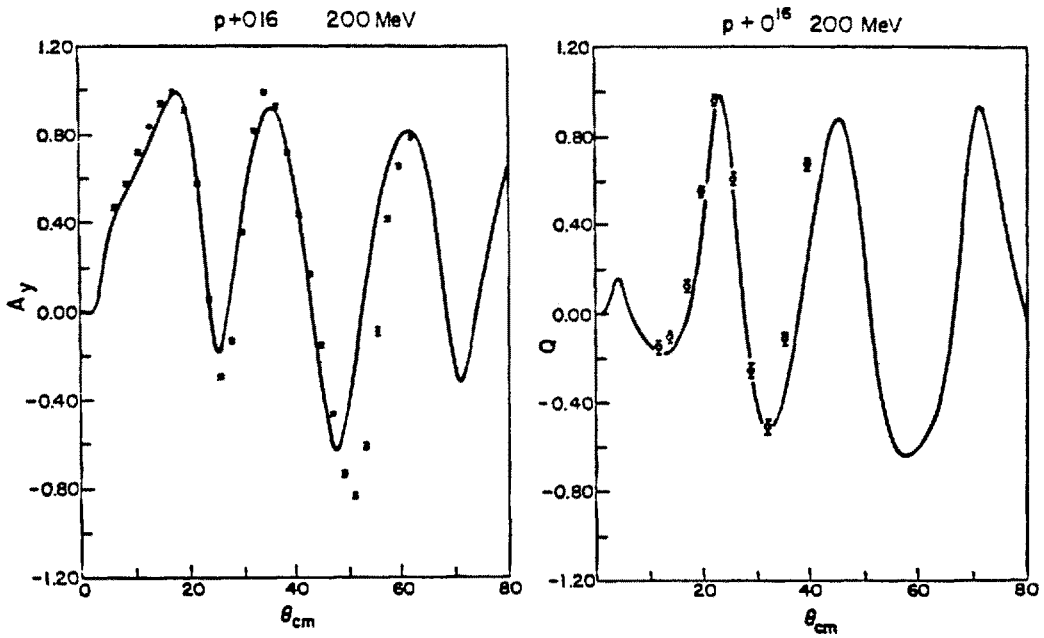

Fig. 5. Spin observalbes for ^{16}O, see Fig. 3. Data from 9, 14.

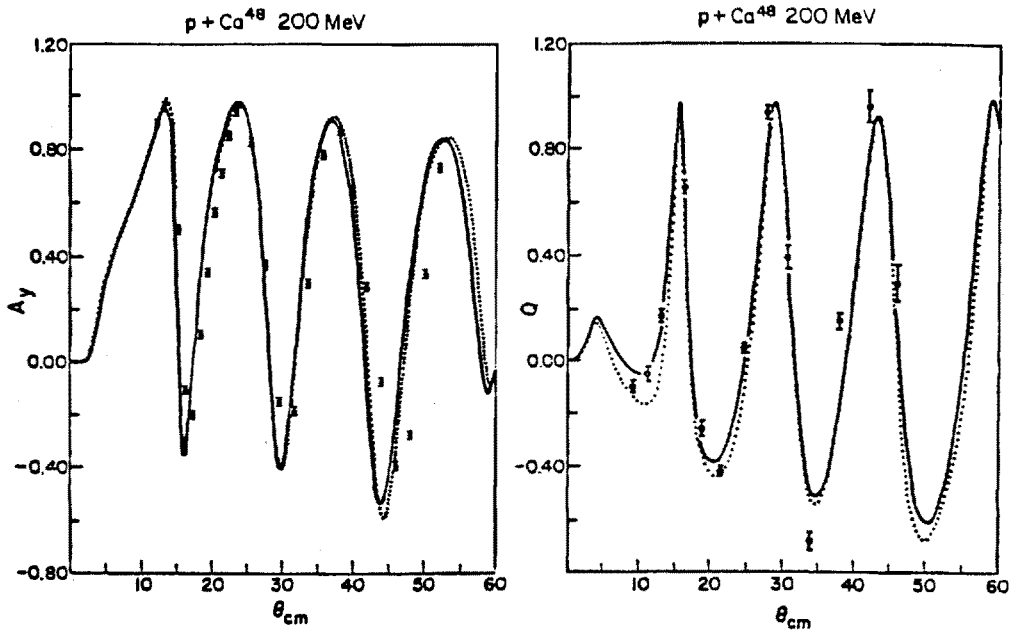

Fig. 6. Spin observables for ^{48}Ca, see Fig. 3. The dotted curve includes a small tensor potential.

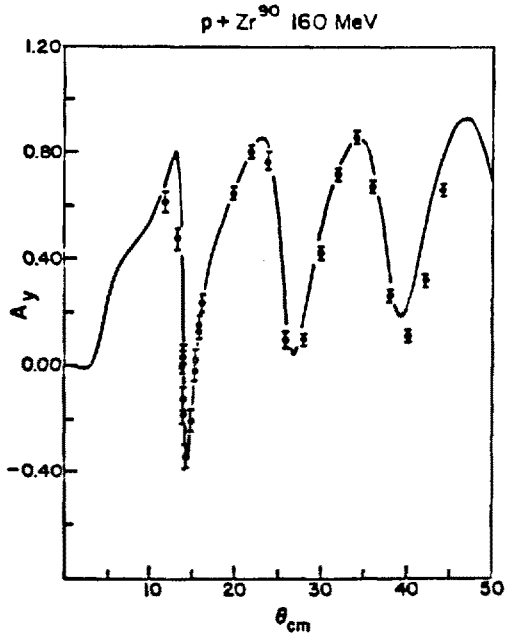

Fig. 7. Analyzing power in ^{90}Zr. The IUCF data is from Ref. [12].

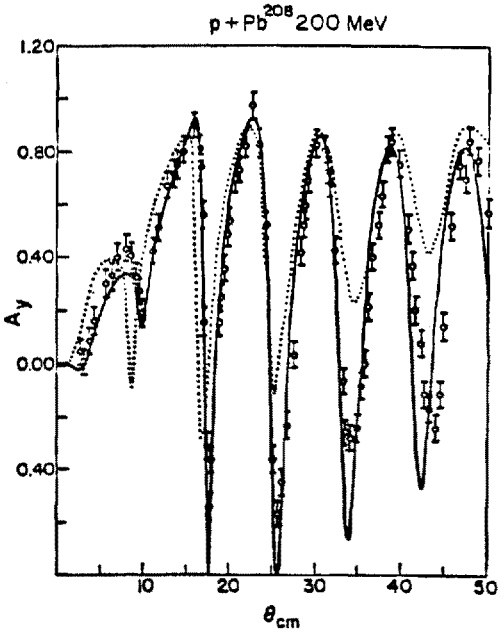

Fig. 8. Analyzing power in ^{208}Pb (solid). The nonrelativistic calculation of [6] is dotted and the TRIUMF data is from [13].

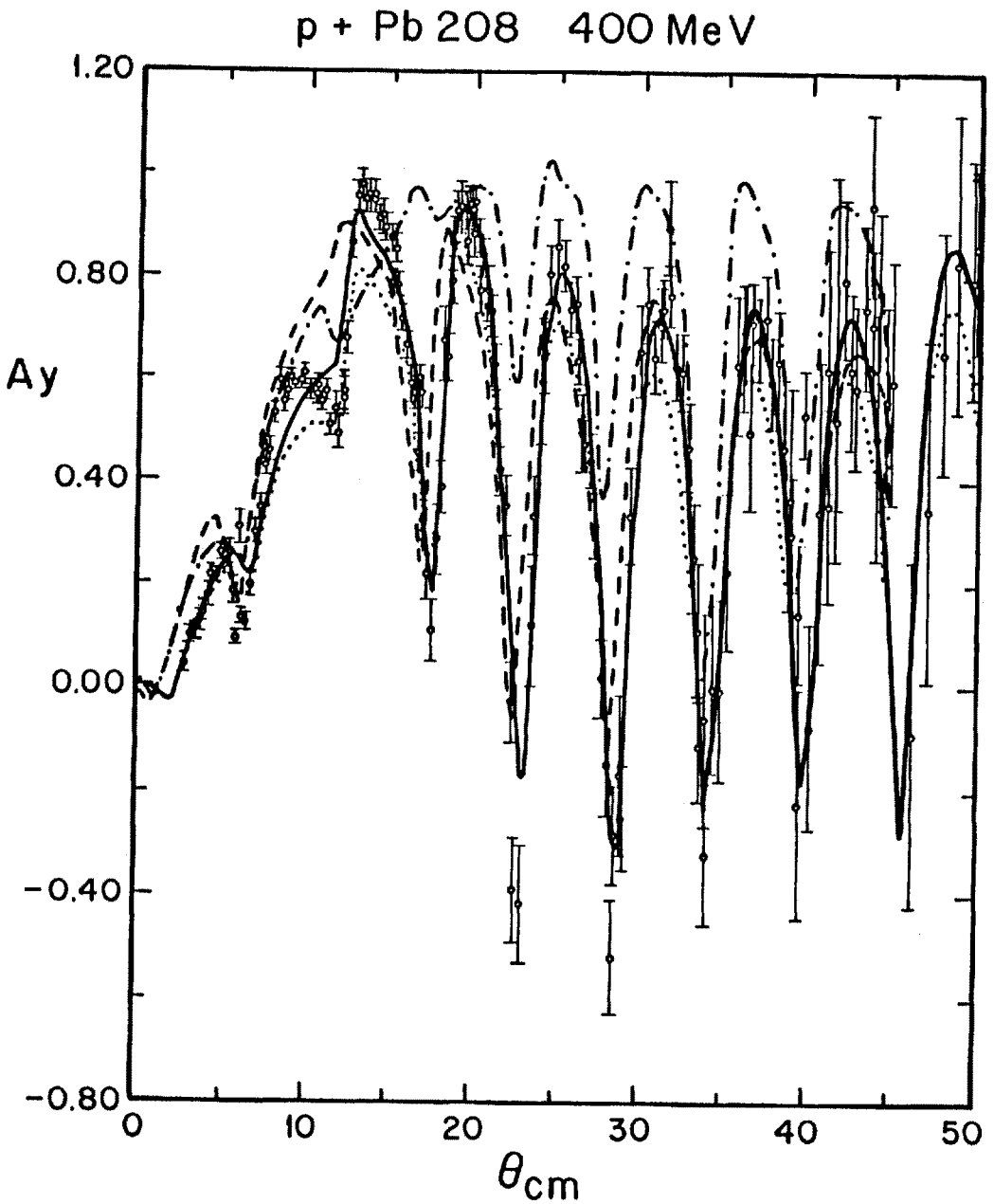

Fig. 9. Analyzing power in ^{208}Pb at 400 MeV (TRIUMF data). Curves with Pauli blocking are solid (relativistic) and dashed (nonrel. from ref [6]). The impulse approx results are dotted (rel.) and dot dashed (nonrel. KMT from ref [16]).

blocking (solid) have only slightly larger maxima then free calculations (dotted). Thus the effects of Pauli blocking while not absent are much smaller then in some nonrelativistic calculations. As the energy increases above 400 MeV the present calculations reduce to the original RIA (which provides an excellent description of data at these energies).

CONCLUSIONS

Microscopic relativistic optical potentials have been calculated for closed shell nuclei at energies near 200 MeV. These calculations go beyond the simple RIA by resolving ambiguities in the relativistic NN amplitudes and including Pauli blocking corrections.

The calculations quantitatively reproduce all measured elastic spin observables (both A_y and Q) for closed shell nuclei at energies near 200 MeV. It remains to be seen how unique this good description is. Further nonrelativistic work to compare with this relativistic approach would be very useful.

ACKNOWLEDGMENTS

Dr. Ed Stevenson is thanked for providing the very nice preliminary IUCF Q data.

REFERENCES

1. C.J. Horowitz and Brian D. Serot, Nucl. Phys., A368:503 (1981).

2. L.G. Arnold, et al., Phys. Rev., C23:1949 (1981); B.C. Clark, et al., Proceedings of "The Interaction Between Medium Energy Nucleons in Nuclei", H.O. Meyer, ed., AIP #97, Bloomington, IA (1982).

3. J.A. McNeil, J. Shepard and S.J. Wallace, Phys. Rev. Lett., 50:1439 (1983; J. Shepard, J.A. McNeil and S.J. Wallace, Phys. Rev. Lett., 50:1443 (1983).

4. C.J. Horowitz, Phys. Rev., C31:1340 (1985).

5. J.A. Tjon and S.J. Wallace, University of Maryland preprint 85-052 (1985), submitted to Phys. Rev. Lett.

6. L. Rikus and H.V. von Germab, Nucl. Phys., A426:469 (1984).

7. J.A. McNeil, L. Ray and S.J. Wallace, Phys. Rev., C27:2123 (1983).

8. K. Holinde, K. Ekelenz and R. Alzetta, Nucl. Phys., A194:161 (1972).

9. E. Stevenson, Proceedings of "Dirac Approaches to Nuclear Physics", Los Alamos (1985), and private communication.

10. B.C. Clark, private communication (1985).

11. F.A. Brieva and J.R. Rook, Nucl. Phys., A291:317 (1977).

12. P. Schwandt, H.O. Meyer, W.W. Jacobs, A.D. Bacher, S.E. Vigdo, M.D. Kaitchuck and T.R. Donoghue, Phys. Rev., C26:55 (1982).

13. D.A. Hutcheon, J.M. Cameron, R.P. Liljestrand, P. Kitching, C.A. Miller, M.J. McDonald, D.M. Shephard, W.C. Olsen, G.C. Neilson, H.S. Sherif, R.N. MacDonald, G.M. Stinson, D.K. McDaniels, J.R. Tinsley, L.W. Swenson, P. Schwandt, C.E. Stronach and L. Ray in: "Polarization Phenomena in Nuclear Physics, G.G. Ohlsen, ed., (1980) (AIP, 1981).

14. C.W. Glover, P. Schwandt, H.O. Meye, W.W. Jacobs, J.R. Hall, M.D. Kaitchuck and R.P. DeVito, Phys. Rev., C31:1 (1985).

15. C.J. Horowitz and B.D. Serot, Phys. Letts., 137B:287 (1984), and to be published.

16. L. Ray and G.W. Hoffman, Phys. Rev. C31:538 (1985).